Available online at www.sciencedirect.com
SCIENCE DIRECT
Journal of Asian Earth Sciences 28 (2006) 81–98
Journal of Asian Earth Sciences
www.elsevier.com/locate/jaes

Petrology, fluid inclusions and metamorphic history of Bhopalpatnam granulites, central India

M. Santosh [a,*], T. Tsunogae [b], T. Iki [a], S. Vansutre [c], K.R. Hari [d]

[a] Faculty of Science, Kochi University, Akebono-cho 2-5-1, Kochi 780-8520, Japan
[b] Institute of Geoscience, University of Tsukuba, Ibaraki 305-8571, Japan
[c] HII/53, Sector I, Pt. Deendayal Upadhyay Nagar, Raipur 492 010, India
[d] Department of Geology, Government Arts and Science College, Durg 491 001, India

Received 17 November 2003; received in revised form 25 May 2004; accepted 15 June 2004

Abstract

The Bhopalpatnam granulite belt (BGB) flanks the Pranhita–Godavari (PG) rift basin with ages ranging from 1.6 to 1.9 Ga, representing a major Mesoproterozoic thermal regime in central India. We present here new results on the metamorphic P–T conditions from garnet-bearing enderbitic charnockite and pelitic gneisses, and document the fluid regimes from detailed fluid inclusions studies in corundum and quartz in corundum-bearing gneiss and garnet–sillimanite–rutile gneiss, respectively, from this granulite belt. A peak pressure–temperature window of 8–9.5 kbar and 720–800 °C is defined by phase equilibrium considerations on garnet–clinopyroxene–plagioclase–quartz assemblages in garnet–bearing charnockite. The garnet–plagioclase–sillimanite–quartz assemblages in pelitic gneiss yield slightly lower P–T estimates of 660–720 °C at 4.7–6.5 kbar.

Primary fluid inclusions in corundum comprise monophase carbonic inclusions with melting temperatures varying from −56.6 to −57.4 °C, indicating that the dominant part of the trapped fluid is pure CO_2. The inclusions homogenize into the liquid phase at temperatures in the range of −18.5 to −5.9 °C (1.024–0.961 g/cm^3). Fluid inclusions in quartz from garnet–sillimanite–rutile gneiss correspond to two categories; Group I (primary) and Group II (pseudosecondary). Both the groups show melting temperatures in the range of −55.9 to −62.9 °C, suggesting the presence of traces of other volatiles (CH_4/N_2) in addition to CO_2. The homogenization temperature of Group I inclusions ranges from −46.3 to −0.1 °C, the extreme low homogenizations indicating very high-density (up to 1.140 g/cm^3) for the carbonic fluid. Group II inclusions show higher homogenization temperatures of up to 16.2 °C. The estimated CO_2 isochore for primary inclusions in corundum and quartz intersects the peak P–T condition of the BGB derived from mineral phase equilibria. We therefore, infer that CO_2 was the dominant fluid species that was trapped at or near the peak metamorphic conditions in BGB. The metamorphic and fluid regimes, as well as the exhumation history of this granulite belt are thus constrained from a combination of petrologic and fluid inclusion studies.

Keywords: Granulite; Petrology; Fluid inclusions; Bhopalpatnam; Central India

1. Introduction

Petrologic, fluid inclusion, and stable isotopic studies on magmatic and metamorphic rocks from various segments of the continental crust have attested to significant fluid movements in the lower crust. Compositional modifications of the deep crust are achieved more effectively by fluids rather than through vapour-absent conditions or dry diffusion process. Fluids are thought to play a significant role in the formation of some of the high-grade metamorphic rocks, particularly those which contain dry granulite assemblages (Touret, 1985, 2001; Touret and Huizenga, 1999). The stabilization of the anhydrous index mineral orthopyroxene in these rocks requires the H_2O-activity to be low during granulite–facies metamorphism. This is because most of the crustal components such as pelitic, psammitic, and granitic rocks would be subjected to hydrous melting at high H_2O-activities during high-grade metamorphism, and anhydrous minerals will not be stabilized. A combination of petrologic and fluid inclusion study in high-grade metamorphic rocks have proved to be one of the important techniques in characterizing metamorphic evolution and fluid regimes (Santosh et al., 2003). In this case, direct

* Corresponding author. Tel./fax: +81 88 844 8278.
E-mail address: santosh@cc.kochi-u.ac.jp (M. Santosh).

1367-9120/$ - see front matter © 2006 Elsevier Ltd. All rights reserved.
doi:10.1016/j.jseaes.2004.06.009

information on the nature, composition, and density of fluids attending metamorphism, which, in conjunction with mineral phase equilibria, yield useful information on the P–T–X conditions and exhumation paths (e.g. Touret, 1985, 2001; Touret and Hansteen, 1988; Bolder-Schrijver et al., 2000; Tsunogae et al., 2002; Santosh et al., 1991, 2003). Recently, Santosh and Tsunogae (2003) reported extremely high-density CO_2-rich fluid inclusions in a late Archaean garnet granulite from southern India, with densities in the range of 1.172–1.155 g/cm^3. These are by far the highest density CO_2-rich fluids yet documented from the continental crust. In most cases, the observation of high-density CO_2-rich fluids is consistent with the low water activities predicted by mineral phase equilibria in these rocks, and suggests that CO_2 could have acted as a potential drying agent.

In this study, granulite-facies rocks from the Bhopalpatnam granulite belt (BGB) in the Bastar Craton in central India were investigated in terms of petrology, P–T conditions, and fluid inclusions. While several reports exist on the high grade rocks in the southern granulite terrain of South India, very limited information is presently available on the petrologic history and fluid regimes in BGB, apart from a previous report by Narasimha et al. (1996). The results of the present study are therefore important in understanding the metamorphism and exhumation histories of the BGB, as well as in evaluating the nature and role of fluids in the mid- to deep-crust.

2. Granulite belts in central India

The Peninsular Indian shield is divisible into two distinct crustal provinces, namely the Southern (SCP) and the Northern crustal province (NCP), which are separated by the central Indian tectonic zone (CITZ, Fig. 1) (Radhakrishna and Naqvi, 1986; Yedekar et al., 1990), characterised by complex Proterozoic crustal history (Acharyya and Roy, 2000; Acharyya, 2003). The SCP consists of three Archaean cratonic nuclei (>3.0 Ga) such as West Dharwar, Bastar and Singhbhum, whereas, the Bundelkhand craton comprises the NCP, The Dharwar, Bastar and Singhbhum cratons are juxtaposed across the NW–SE trending Pranhita–Godavari (PG) and Mahanadi rift basins (Fig. 1). The latter largely hosts Late Paleozoic–Mesozoic Gondwana sediments with no evidence as yet for Proterozoic activity, whereas the PG basin exposes Proterozoic and Gondwana sediments.

Two important granulite belts, namely the Karimnagar granulite belt (KGB) and the Bhopalpatnam granulite belt (BGB) occur along both flanks of the Pranhita–Godavari (PG) rift basin (Rajesham et al., 1993; Acharyya, 1997,

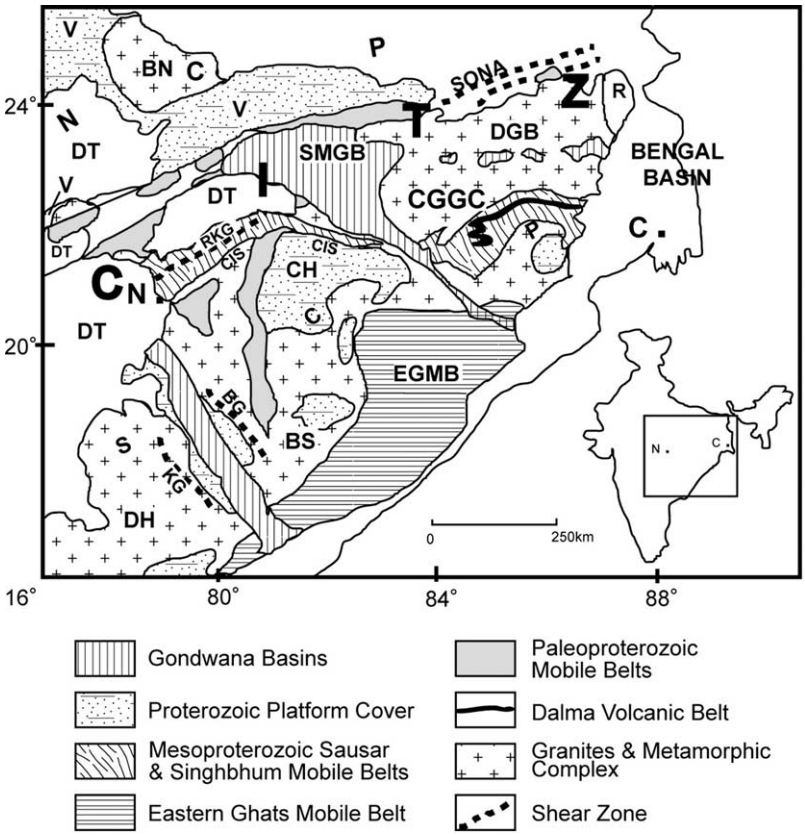

Fig. 1. Geological map of a part of Peninsular India (modified after Acharyya, 2003). Archaean cratons: BS, Bastar; BN, Bundelkhand; DH, Dharwar; SN, Singhbhum. Basins: CH, Chhattisgarh Basin; DGB, Damodar Gondwana Basin; PGB, Pranhita, Godavari Basin; SMGB, Son Mahanadi Gondwana Basin; V, Vindhyan Basin. Granulite Belts: BG, Bhopalpatnam Granulite Belt; Balaghat, Bhandara Granulite Belt; developed along some parts of the CIS, Central Indian Shear Zone; KG, Karimnagar Granulite Belt; RKG, Ramakona–Katangi Granulites. Abbreviated localities: C, Calcutta; N, Nagpur. Others: CITZ (shown detached in bold letters), Central Indian Tectonic Zone; DT, Deccan Trap; EGMB, Eastern Ghats Mobile Belt; NCP, Northern Crustal Province; SCP, Southern Crustal Province; CGGC, Chotanagpur Gneissic Complex; SONA, Son-Narmada Lineament (figure after Santosh et al., 2004).

2000; Mishra et al., 1999; Santosh et al., 2004). Although a third one—the Sausar Mobile Belt (SMB)—is also an important member of the central Indian granulite belts, it belongs to the NCP. The KGB is inferred to represent a remnant of an Archaean supracrustal–granite association which underwent granulite grade metamorphism at ~2.5 Ga (Rajesham et al., 1993). Tectonothermal event in KGB match with that of East Dharwar craton, which is regarded as a separate entity. A recent geochronological study of the BGB rocks based on EPMA dating of zircon and monazite from granulite grade lithologies (Santosh et al., 2004) has aided in elucidating the tectonic history of this granulite belt. Zircons from BGB have 1.9 Ga cores mantled by 1.7 Ga rims. Zircons with core ages of 1.6–1.7 Ga in BGB rocks suggest new growth at this time. Monazites from BGB define sharp linear trend in PbO vs. ThO_2^* diagram delineating a clear isochron with age of 1.59 ± 0.03 Ga. Age data from BGB and KGB (cf. Santosh et al., 2004) negate current models linking these terrains to 'Godavari Granulite Belt' and considering them as single and contemporaneous entity. The mid Archaean to early Palaeoproterozoic signature recognized from KGB is totally missing in BGB. On the other hand, KGB rocks do not record any evidence for major Mesoproterozoic thermal regime. The two granulite belts shouldering the PG rift basin might have therefore evolved in different times under distinct P–T conditions and thermal regimes. While tectonothermal events in KGB broadly match with those of East Dharwar, the BGB represents a mobile belt that was incorporated in a collisional zone between Bastar and Dharwar cratons. The mid Archaean ages from KGB rocks indicate that the terrain was part of the East Dharwar craton and a component of the old continental assembly of Ur (cf. Rogers and Santosh, 2003). The 1.6 Ga mobile belt at the collision margin between the Dharwar and the Bastar cratons, superposed by rift activity along the PG basin at 1.5 Ga, closely match with the history of accretion and break-up of the supercontinent Columbia (cf. Rogers and Santosh, 2002). Lack of any Grenville ages (1.0 Ga) corresponding to the Rodinia accretion or late Pan-African ages (ca. 550 Ma) relating to the Gondwana amalgamation indicate that the PG basin did not witness any of these younger events.

3. Bhopalpatnam granulite belt

The Bhopalpatnam granulite belt occurs along the SW margin of the Bastar craton and NE shoulder of the PG rift basin and extends ca. 300 km in length and ca. 20–40 km in width (Fig. 2) (Mishra et al., 1988; Narasimha et al., 1996). The eastern margin of BGB is characterized by the 'opx- in' isograd indicated by the appearance of opx. The lithologic association in this region includes younger granite, two-pyroxene granulite, Ol–Spl–Opx bearing ultramafics, charnockite and charnockitic gneiss of tonalite-trondhjemitic affinity, enderbite, quartzite, calc–silicate, Al– and Mg–Al pelite, BIF, and gneiss-migmatites. The association has striking continental margin affinities. The pelite and carbonate lithologies posses assemblages like Crd–Grt–Sil–Bt–Rt–Ilm–Kfs–Pl–Spl–Qtz, Wo–Scp–Cal–Di–Adr–Grs and Grt–Pl–Qtz–Mag, based on which P–T conditions of metamorphism were estimated to range from 6 to 9 kbar at 750 °C with an initial IBC path (Narasimha et al., 1996). An assemblage of Qtz–Crd–Spl–Spr–Crn–Pl–Sil–Grt–Op–Bt–Zrn is recorded from Mg–Al metapelite. The presence of sapphirine in the assemblage indicate very high P–T condition, with T > 800 °C at $P = 8$–10 kbar (Ramachandra et al., 2001; symbols for minerals and mineral abbreviations used in text are after Kretz, 1983).

The major lithounits in BGB, SE of Bhopalpatnam investigated in this study include Grt–Cpx ± Opx bearing enderbitic charnockites, Grt–Bt ± Sil gneiss and Grt-Sil-Rt-gneiss with corundum. In the study area, charnockites, amphibolites, garnet–biotite gneiss, and garnet–sillimanite gneiss carrying corundum and rutile are exposed. Coarse semi-precious corundum crystals are locally mined in the area. EPMA zircon and monazite ages ranging from 1.6 to 1.9 Ga reported in Santosh et al. (2004) were obtained from enderbitic charnockite, garnet–biotite gneiss and garnet–sillimanite–rutile metapelites from this area, correlating the granulite facies metamorphism in the study area with a major Mesoproterozoic thermal event.

4. Petrography and mineral chemistry

Petrographic studies including mineral assemblages, textures, grain size measurements were performed using a petrological microscope. The mineral assemblages in the rocks examined in this study are given in Table 1. Representative photomicrographs of the mineral assemblages in various rock types are shown in Fig. 3.

Chemical analyses of minerals were performed by electron microprobe analyzer at Kochi University (Japan) and at Rand Afrikaans University (South Africa). At Kochi University, the analyses were performed using EPMA Model JEOL JXA-8600S/M at an accelerating voltage of 15 kV, specimen current of 10 nA and beam diameter of 1 μm. Mineral analyses at RAU, South Africa were performed by Oxford EDS instrument under conditions of 15 kV accelerating voltage and 10 nA sample current, and the data were regressed using ZAF correction. Representative compositions of minerals in the analyzed samples are given in Table 2.

4.1. Charnockite (samples K-14 and K-3)

The charnockite in the study area is of enderbitic variety and occurs as a thick band of ca. 200 m width within garnet–biotite gneiss. The rock comprises mainly of plagioclase, clinopyroxene, calcic amphibole, and garnet. Orthopyroxene occurs in some places. Quartz is present as an accessory mineral. Foliation of the rock is not obvious under thin section or hand specimen, while lineation is clearly defined by plagioclase-rich grayish patches, as will be discussed later.

Garnet (0.4–2.9 mm) is sub- to anhedral and is almandine-rich in composition (Alm_{59} Pyr_{19} Grs_{20} Sps_2). The garnet grains do not exhibit any marked compositional zoning.

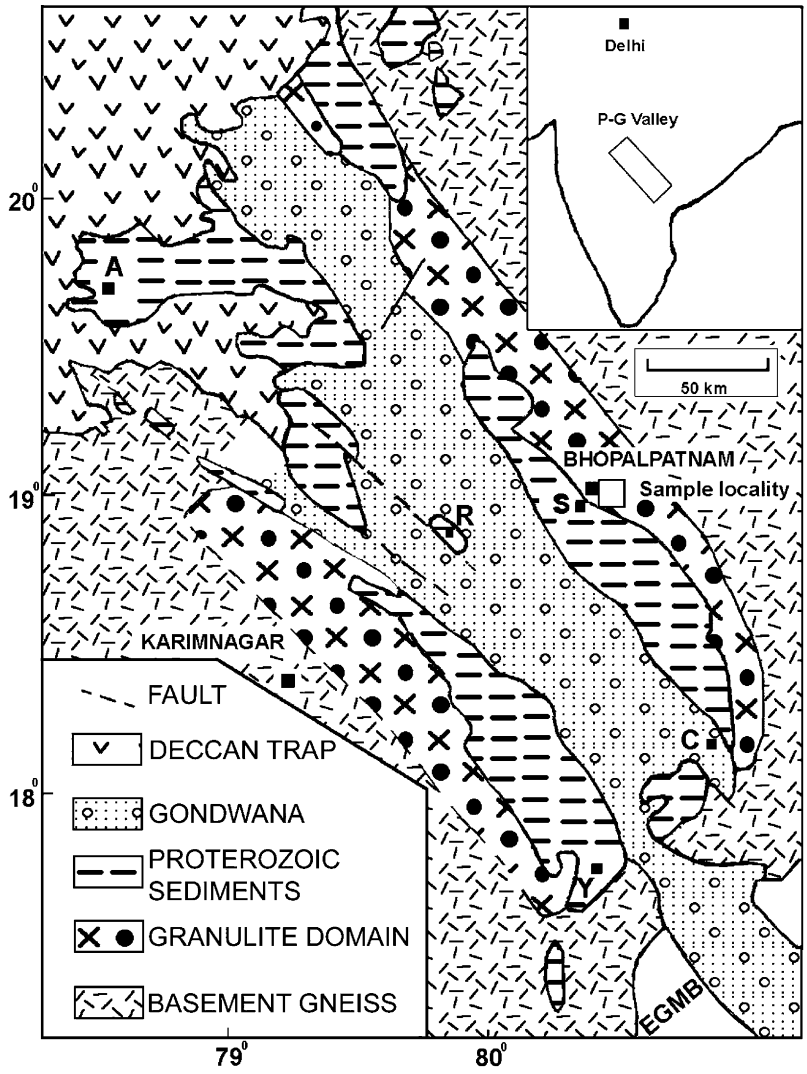

Fig. 2. Geological map of Bhopalpatnam and Karimnagar Granulite Belts, and P–G Basin (modified after Ramachandra et al., 2001). Location of samples shown. Abbreviated localities: A, Adailabad; C, Cherla; R, Rajul Gutta; S, Somanpalli; Y, Yellandapad.

Clinopyroxene (0.2–1.6 mm) is subhedral and is salite in composition (X_{Mg} = Mg/(Fe + Mg) = 0.66). Plagioclase ($An_{45–47}$) occurs as medium-grained (0.2–0.9 mm) aggregates defining felsic-rich domains in the rock. The mineral also occurs within domains that are present as elongated grayish patches of about 5 × 3 mm scattered in dark-brownish matrix composed mainly of plagioclase, garnet, and clinopyroxene. There is no significant difference in grain size and chemistry of plagioclase between the plagioclase-rich and matrix portions. Calcic amphibole (0.3–3.3 mm) is present as a minor constituent in plagioclase-rich patches or as matrix aggregates. It is compositionally pargasite to tschermakite (X_{Mg} = 0.55–0.57, $(Na + K)_A$ = 0.49–0.54, Si = 6.27–6.30 pfu) according to the classification of Leake et al. (1997). The Fe^{3+} content is small as $Fe^{3+}/(Fe^{2+} + Fe^{3+}) < 0.2$, if we apply the recalculation method of 13eCNK (13 cations excluding Ca, Na, and K). Compositional variation of amphibole chemistry is negligible. Rarely, medium- to fine-grained (< 0.5 mm) calcic amphibole occurs as inclusions in clinopyroxene, suggesting that a prograde dehydration reaction took place.

Table 1
Mineral assemblage in Bhopalpatnam granulites

Sample No.	Rock type	Minerals
K10	Corundum bearing gneiss	Corundum + biotite + sillimanite + plagioclase + K-feldspar
K11	Garnet Sillimanite gneiss	Garnet + biotite + plagioclase + k-feldspar + sillimanite + quartz + rutile
K21		Garnet + biotite + plagioclase + k-feldspar + sillimanite + quartz + rutile
K14	Charnockite	Garnet + clinopyroxene + (−)orthopyroxene + hornblende + plagioclase + quartz
K3		Garnet + clinopyroxene + (−)orthopyroxene + hornblende + plagioclase + quartz

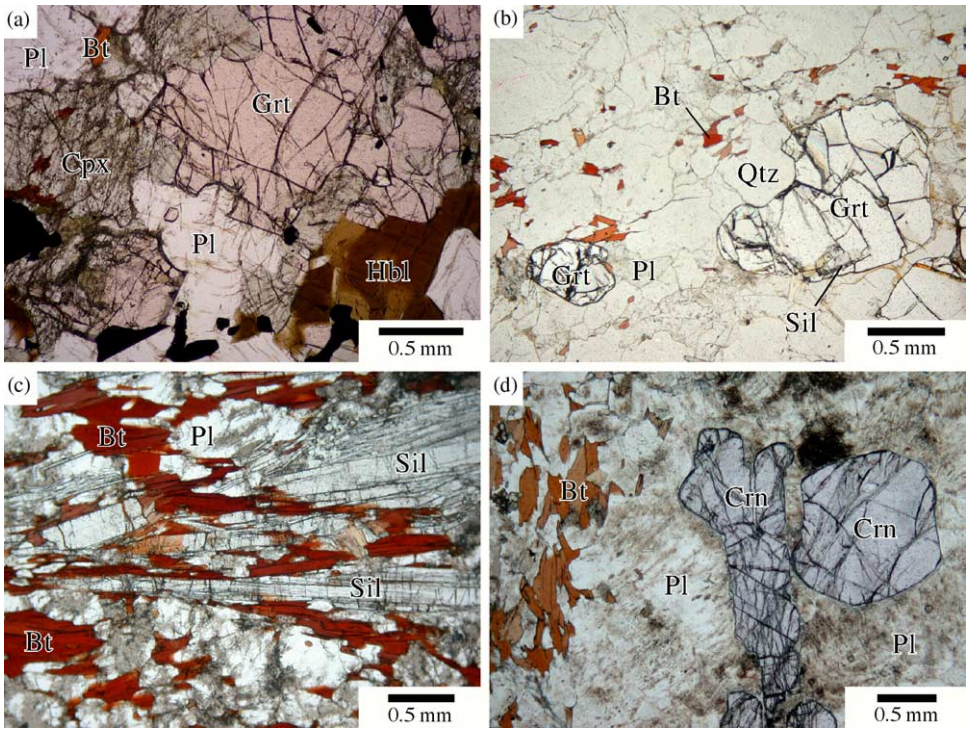

Fig. 3. Photomicrographs showing mineral assemblages from representative lithologies in the Bhopalpatnam granulite belt. Mineral abbreviations are after Kretz (1983). (a) Garnet–clinopyroxene–pargasite–plagioclase assemblage in enderbetic charnockite (sample K-14). (b) Foliated biotite and sillimanite assemblage in pelitic gneiss (sample K-11). (c) Garnet–biotite–sillimanite assemblage in pelitic gneiss (sample K-20). (d) Coarse-grained corundum in altered plagioclase-biotite aggregates in sample K-10A.

4.2. Pelitic gneiss (samples K-11 and K-21)

Pelitic gneiss is the dominant lithology in the study area. Two samples of pelitic gneiss were examined in detail. Sample K-11 is composed of biotite, sillimanite, plagioclase ($An_{34–36}$), quartz, and K-feldspar ($Or_{89–94}$). The sample is characterized by lineated prismatic sillimanite (0.1–1.8 mm) along foliation plane. The sillimanite is close to the ideal composition of Al_2SiO_5, although minor Fe (up to 0.01 pfu) is identified. Biotite (0.1–1.2 mm) is also distributed parallel to sillimanite, suggesting their early origin probably around peak metamorphism. Quartz and feldspars (0.1–1.1 mm) are distributed throughout the sample filling matrix of sillimanite and biotite grains.

In contrast, sample K-21 is quartzo-feldspathic and composed mainly of quartz, plagioclase, K-feldspar, garnet, biotite, sillimanite, and rutile. Zircon and monazite are accessory minerals. Similar to sample K-11, the sample is characterized by linear needles of sillimanite (0.05–0.5 mm), biotite (0.05–1.4 mm), and garnet (0.4–3.5 mm), although foliation is not obvious. Fine-grained (0.02–0.15 mm) sillimanite inclusions in garnet are also elongated parallel to matrix sillimanite. Yellowish rutile (0.05–0.20 mm) occurs scattered as well as parallel to the lineation. Its composition is close to pure TiO_2. Poikiloblastic garnet is Fe-rich as Alm_{60} Pyr_{35} Grs_4 Sps_1, and compositionally homogeneous. Biotite composition ($X_{Mg}=0.67–0.68$, $Al^{iv}=2.51–2.53$) is similar to that in sample K-11 ($X_{Mg}=0.65–0.67$, $Al^{iv}=2.50–2.60$), but it is characterized by higher TiO_2 content (up to 4.9 wt%) than the biotite in sample K-21 (2.9–3.2 wt%). Sillimanite contains minor Cr and Fe, although they total less than 0.01 wt%.

4.3. Aluminous gneiss (sample K-10)

Thin layers of corundum-bearing aluminous gneiss occur within dominantly pelitic gneiss that trend as large bands of a few hundred meters thickness. This rock type is compositionally pelitic, but characterized by the presence of abundant corundum (more than 5 vol%). Sample K-10A is composed of plagioclase ($An_{31–38}$), biotite, K-feldspar ($Or_{90–93}$), sillimanite, and corundum. Quarts is absent in the sample. Chlorite and sericite occur as secondary minerals.

Coarse-grained (up to 17 mm) corundum is present only in plagioclase-rich leucocratic portion of the sample, and surrounded by aggregate of plagioclase (0.2–1.0 mm) and minor biotite. It is compositionally nearly pure Al_2O_3, with minor Cr_2O_3 (up to 0.3 wt%) and Fe_2O_3 (up to 0.1 wt%). No reaction textures have been identified around the corundum grains. Biotite (0.2–1.0 mm) is rich in Mg ($X_{Mg}=0.81–0.82$) and poor in Ti ($TiO_2=1.5–1.9$ wt%) compared to that in pelitic gneisses. It occasionally coexists with K-feldspar (0.3–1.4 mm, $Or_{90–93}$) and sillimanite (0.2–4.0 mm). The sillimanite composition is close to Al_2SiO_5 similar to that in samples K-11 and K-21.

Table 2
Representative electron microprobe data on granulite facies assemblages from Bhopalpatnam

Sample No.	K-14 (charnockite)							K-3 (charnockite)					
Mineral name	Grt	Grt	Cpx	Cpx	Pl	Hbl	Hbl	Grt	Grt	Cpx	Pl	Hbl	Hbl
O[a]	12	12	6	6	8	23	23	12	12	6	8	23	23
	Core	Rim	Core	Rim	Core	Core	Core	Core	Rim	Core	Core	Core	Core
SiO_2	38.74	38.58	51.35	51.20	56.55	42.22	42.43	38.61	38.33	50.84	56.96	42.22	42.12
Al_2O_3	21.58	21.68	1.83	1.70	27.56	12.02	12.38	21.76	21.65	2.09	27.48	12.01	12.04
TiO_2	0.19	0.08	0.26	0.22	0.00	2.50	3.15	0.09	0.09	0.27	0.00	2.46	2.63
Cr_2O_3	0.04	0.11	0.00	0.00	0.00	0.30	0.08	0.03	0.00	0.03	0.00	0.04	0.00
FeO[b]	26.68	27.78	11.88	13.17	0.09	16.78	16.89	26.32	28.16	12.38	0.13	16.73	16.43
MnO	1.08	1.22	0.28	0.24	0.00	0.21	0.07	1.38	0.94	0.20	0.04	0.13	0.04
MgO	4.72	4.27	11.95	11.95	0.00	9.66	9.66	4.91	5.14	11.48	0.00	9.27	9.41
CaO	7.08	6.71	21.89	21.04	9.70	11.19	11.03	6.90	6.79	21.78	9.71	10.65	10.90
Na_2O	0.00	0.00	0.22	0.21	6.12	1.74	1.82	0.03	0.04	0.41	6.08	1.50	1.50
K_2O	0.00	0.00	0.00	0.00	0.23	1.11	1.19	0.00	0.00	0.00	0.23	1.16	1.20
Total	100.10	100.42	99.65	99.73	100.24	97.74	98.69	100.03	101.13	99.47	100.62	96.15	96.26
Si	3.023	3.015	1.951	1.951	2.537	6.356	6.318	3.013	2.980	1.941	2.545	6.436	6.410
Al	1.984	1.997	0.082	0.076	1.457	2.132	2.172	2.001	1.983	0.094	1.447	2.156	2.159
Ti	0.011	0.005	0.008	0.006	0.000	0.283	0.352	0.005	0.005	0.008	0.000	0.281	0.301
Cr	0.003	0.007	0.000	0.000	0.000	0.036	0.009	0.002	0.000	0.001	0.000	0.004	0.000
Fe^{2+}	1.741	1.815	0.377	0.419	0.003	2.112	2.102	1.717	1.830	0.395	0.005	2.132	2.090
Mn	0.071	0.080	0.009	0.008	0.000	0.027	0.009	0.091	0.062	0.006	0.001	0.016	0.005
Mg	0.549	0.497	0.676	0.678	0.000	2.167	2.143	0.571	0.595	0.653	0.000	2.105	2.134
Ca	0.592	0.562	0.890	0.859	0.466	1.803	1.758	0.577	0.565	0.890	0.465	1.739	1.776
Na	0.000	0.000	0.016	0.016	0.532	0.508	0.526	0.004	0.005	0.030	0.526	0.443	0.442
K	0.000	0.000	0.000	0.000	0.013	0.212	0.226	0.000	0.000	0.000	0.013	0.225	0.233
Total	7.973	7.978	4.009	4.013	5.007	15.636	15.615	7.982	8.026	4.019	5.001	15.537	15.548
Mg/(Fe+Mg)	0.240	0.215	0.642	0.618	–	0.506	0.505	0.250	0.245	0.623	–	0.497	0.505

Sample No.	K-11 (pelitic gneiss)						K-21 (pelitic gneiss)						
Mineral name	Bt	Bt	Pl	Pl	Kfs	Sil	Grt	Grt	Bt	Pl	Pl	Kfs	Sil
O[a]	22	22	8	8	8	5	12	12	22	8	8	8	5
	With Sil	With Pl	Core	Rim	Core	Core	Core	Rim	Core	Core	Rim	Core	Core
SiO_2	36.77	37.19	59.22	59.22	63.58	62.34	39.49	39.70	37.17	58.98	58.95	63.55	37.55
Al_2O_3	18.01	17.75	26.47	26.51	19.03	37.80	22.29	22.73	16.81	25.13	25.59	18.74	62.39
TiO_2	3.00	2.89	0.00	0.00	0.00	0.14	0.00	0.04	4.69	0.00	0.00	0.00	0.10
Cr_2O_3	0.42	0.65	0.18	0.00	0.00	0.37	0.10	0.00	0.20	0.00	0.00	0.00	0.21
FeO[b]	12.85	12.57	0.00	0.00	0.35	0.35	27.87	28.24	12.59	0.00	0.00	0.00	0.32
MnO	0.23	0.23	0.00	0.00	0.00	0.00	0.48	0.30	0.00	0.00	0.02	0.00	0.03
MgO	14.11	14.14	0.02	0.00	0.00	0.00	9.19	9.05	14.46	0.00	0.00	0.00	0.00
CaO	0.00	0.00	7.84	7.86	0.00	0.01	1.44	1.38	0.00	6.97	6.94	0.00	0.00
Na_2O	0.00	0.00	7.60	7.70	0.69	0.00	0.00	0.00	0.00	7.80	8.09	1.45	0.00
K_2O	9.93	9.77	0.28	0.21	15.64	0.00	0.00	0.00	9.67	0.27	0.21	14.45	0.00
Total	95.32	95.19	101.60	101.50	99.28	101.01	100.85	101.43	95.60	99.15	99.80	98.19	100.59
Si	5.441	5.496	2.612	2.613	2.962	1.620	3.010	3.006	5.467	2.657	2.641	2.976	1.009
Al	3.141	3.091	1.376	1.378	1.045	1.157	2.002	2.028	2.914	1.334	1.351	1.034	1.976
Ti	0.334	0.321	0.000	0.000	0.000	0.003	0.000	0.003	0.519	0.000	0.000	0.000	0.002
Cr	0.049	0.076	0.006	0.000	0.000	0.008	0.006	0.000	0.023	0.000	0.000	0.000	0.004
Fe^{2+}	1.589	1.553	0.000	0.000	0.014	0.008	1.776	1.788	1.548	0.000	0.000	0.000	0.007
Mn	0.029	0.028	0.000	0.000	0.000	0.000	0.031	0.019	0.000	0.000	0.001	0.000	0.001
Mg	3.110	3.114	0.001	0.000	0.000	0.000	1.044	1.021	3.167	0.000	0.000	0.000	0.000
Ca	0.000	0.000	0.370	0.371	0.000	0.000	0.117	0.112	0.000	0.336	0.333	0.000	0.000
Na	0.000	0.000	0.649	0.658	0.062	0.000	0.000	0.000	0.000	0.681	0.703	0.132	0.000
K	1.873	1.842	0.016	0.012	0.929	0.000	0.000	0.000	1.814	0.015	0.012	0.863	0.000
Total	15.567	15.521	5.030	5.033	5.011	2.795	7.986	7.977	15.452	5.024	5.041	5.005	2.999
Mg/(Fe+Mg)	0.662	0.667	1.000	–	–	0.000	0.370	0.364	0.672	–	–	–	–

Sample No.	K-10 (aluminous gneiss)						
Mineral name	Bt	Bt	Pl	Pl	Kfs	Crn	Sil
O[a]	22	22	8	8	8	3	5
	With Crn	With Sil	With Crn	With Sil	With Sil	Core	Core
SiO_2	38.30	38.45	57.92	57.58	63.93	0.09	37.08
Al_2O_3	18.26	18.73	26.60	26.56	18.86	100.09	62.70

Table 2 (*continued*)

Sample No.	K-10 (aluminous gneiss)						
TiO_2	1.84	1.48	0.07	0.04	0.18	0.08	0.08
Cr_2O_3	0.12	0.31	0.08	0.00	0.24	0.31	0.32
FeO[b]	7.63	7.10	0.00	0.00	0.00	0.02	0.12
MnO	0.20	0.29	0.00	0.02	0.00	0.00	0.05
MgO	18.52	18.51	0.00	0.00	0.04	0.00	0.01
CaO	0.00	0.00	8.23	8.19	0.00	0.00	0.00
Na_2O	0.00	0.00	7.09	7.29	0.79	0.02	0.07
K_2O	9.94	9.66	0.29	0.18	15.67	0.05	0.00
Total	94.82	94.52	100.27	99.87	99.72	100.65	100.42
Si	5.533	5.546	2.590	2.586	2.963	0.002	0.998
Al	3.109	3.185	1.401	1.406	1.030	1.992	1.989
Ti	0.200	0.160	0.002	0.001	0.006	0.001	0.002
Cr	0.014	0.036	0.003	0.000	0.009	0.004	0.007
Fe^{2+}	0.922	0.856	0.000	0.000	0.000	0.000	0.003
Mn	0.025	0.035	0.000	0.001	0.000	0.000	0.001
Mg	3.987	3.977	0.000	0.000	0.003	0.000	0.000
Ca	0.000	0.000	0.394	0.394	0.000	0.000	0.000
Na	0.000	0.000	0.614	0.634	0.071	0.001	0.004
K	1.832	1.776	0.017	0.010	0.927	0.001	0.000
Total	15.622	15.572	5.021	5.032	5.010	2.000	3.004
Mg/(Fe + Mg)	0.812	0.823	–	–	–	–	–

[a] Number of oxygens.
[b] Total Fe as FeO.

5. Geothermobarometry

The granulite samples examined in this study contain several equilibrium assemblages and mineral pairs that are suitable for the application of a number of mineral phase equilibria geothermobarometers. The summary of pressure–temperature computations from mineral chemistry data is briefly discussed below.

5.1. Charnockite (samples K-14 and K-3)

The coexisting garnet–clinopyroxene pairs in samples K-14 and K-3 provide robust geothermometers. Application of the method of Ellis and Green (1979) yields a temperature range of 740–810 °C at 8 kbar (pressure estimate discussed below). The method is based on experimental calibration of Fe–Mg cation partitioning between garnet and clinopyroxene in eclogites at 750–1300 °C and 24–30 kbar. In this calibration, the distribution coefficient is dependent upon Ca contents and apparently independent of the Mg/(Fe + Mg) ratios of the minerals. Computations based on Powell (1985); Sengupta et al. (1989) techniques yield 720–790 °C and 800–870 °C, respectively, and are similar to the results obtained from the calibration of Ellis and Green (1979). The two methods are improvised versions of the Ellis and Green (1979) technique.

However, garnet–clinopyroxene temperatures computed from the techniques of Pattison and Newton (1989); Ai (1994) show slightly lower values (640–740 and 650–720 °C, respectively) which seem to be unrealistically low for the peak metamorphic conditions of the pyroxene-bearing rock. Considering the effect of retrograde Fe–Mg re-equilibration following peak metamorphism (e.g. Frost and Chacko, 1989), these low temperatures cannot be neglected and could possibly indicate the lower limit of high-grade metamorphism.

Temperatures were also computed from hornblende-plagioclase geothermometer of Holland and Blundy (1994). Application of this calibration yielded 770–820 °C in sample K-14 and 710–780 °C in sample K-3, both estimates at 6 kbar (average pressure estimate, see below). The temperature estimates on charnockite samples from the garnet–clinopyroxene thermometer and hornblende-plagioclase thermometer are closely comparable within limits of computational error. Slightly lower temperature range was obtained from garnet–hornblende geothermometer of Graham and Powell (1984) as 700–730 °C.

The presence of the equilibrium assemblage garnet–clinopyroxene–plagioclase–quartz in the sample offers a reliable geobarometer. Perkins and Newton (1981) and Newton and Perkins (1982) proposed a geobarometer using the following equilibrium reaction (1) based on available thermodynamic data:

$$\underset{\text{diopside}}{CaMgSi_2O_6} + \underset{\text{anorthite}}{CaAl_2Si_2O_8} = \underset{\text{grossular}}{2/3Ca_3Al_2Si_3O_{12}} + \underset{\text{pyrope}}{1/3Mg_3Al_2Si_3O_{12}} + \underset{\text{quartz}}{SiO_2} \quad (1)$$

Application of this geobarometer for the reaction (1) in the sample yields a pressure range of 6.0–6.3 kbar at 800 °C. On the other hand, slightly higher pressure range of 8.2–8.5 kbar was obtained from garnet–hornblende–plagioclase–quartz geobarometer of Kohn and Spear (1990).

5.2. Pelitic gneiss (sample K-21)

The garnet–biotite and garnet–plagioclase–sillimanite–quartz assemblages in the sample were used for computing geothermometry and geobarometry, respectively. The Fe–Mg exchange between garnet and biotite is widely used as a geothermometer. Numerous experiments and empirical calibrations between the two mineral pairs have been done so far to construct reliable geothermometers. However, application of garnet–biotite geothermometers to granulite-facies rocks generally yield temperature values lower than those obtained by other methods such as garnet–orthopyroxene and garnet–clinopyroxene pairs. This is mainly due to the retrograde cation exchange reaction and, therefore, the garnet–biotite pairs in granulite-facies rocks often preserve only the retrograde metamorphic conditions. Experimentally determined methods of Holdaway and Lee (1977); Perchuk and Lavrent'eva (1983) have been adopted in this study. Application of the two methods to the equilibrium garnet–biotite pairs in the sample yielded the temperature ranges of 690–720 and 660–690 °C at 7 kbar. Other garnet–biotite geothermometric calibrations give similar or slightly lower temperature values.

Garnet–plagioclase–sillimanite–quartz geobarometer is commonly used for estimating pressures in pelitic rocks. The calibration follows the reaction:

$$\underset{\text{anorthite}}{3CaAl_2Si_2O_8} = \underset{\text{grossular}}{Ca_3Al_2Si_3O_{12}} + \underset{\text{sillimanite}}{2Al_2SiO_5} + \underset{\text{quartz}}{SiO_2} \quad (2)$$

Newton and Haselton (1981) calibrated the geobarometer based on available experimental data of the reaction. On the other hand, Ganguly and Saxena (1984) evaluated the non-ideality of garnet and plagioclase in the reaction, and determined empirical correction parameters for the barometer. Application of the above methods yielded pressure values of 5.5–5.8 and 5.6–6.3 kbar, respectively, at 700 °C.

6. Fluid inclusion petrography

6.1. Method of investigation

Fluid inclusions were studied in doubly polished thin wafers of representative samples; i.e. corundum-bearing gneiss (sample K-10), charnockite (samples K-3 and K-14), and garnet–sillimanite–rutile gneiss (samples K-21). The nature of occurrence of inclusions, their distribution pattern, shape, size and phase categories were carefully studied and documented under a petrological microscope at varying magnifications following the techniques outlined by Roedder (1984). Touret (2001), and Van den Kerkhof and Hein (2001). In general, fluid inclusions were observed to be present in different minerals in all the examined samples, although their size, relative abundance, and distribution pattern vary among the different rocks. Fluid inclusion studies were carried out on the same representative samples, on rock wafers from the same portions of samples that were used for petrologic and mineral phase equilibria investigations. The charnockite samples contained fluid inclusions in garnet, but these inclusions were mostly dark and phase changes, if any, were difficult to observe during heating–freezing studies. Therefore, these are not further discussed in this report. The results from inclusion petrography discussed below are from corundum within corundum-bearing gneisses and quartz from garnet–sillimanite–rutile gneisses.

6.2. Results

6.2.1. Fluid inclusions in corundum

Some of the corundum grains examined contain numerous fluid inclusions of various sizes and shapes. Their sizes range from less than 5–30 μm. Most of them are between 15 and 25 μm in size. Some rare inclusions are larger, and more than 30 μm in size. They show diamond-shaped, ovoid, rounded, elongate, needle-shaped or irregular cavities. The most common category is flat and tabular inclusions showing elongate and regular cavities (Fig. 4a). Because of the internal reflection from the three dimensional inclusion cavities, some inclusions show parting-like textures, and mimic the structure of the host mineral. The preferred alignment of many inclusions with long axis parallel to the *c*-axis of the crystal indicates a direct control of the crystallography of the host corundum with the entrapment of inclusions.

A second generation of inclusions shows highly irregular and elongate cavities that are interconnected in a 'web'-like fashion (Fig. 4b), which appear to be pseudosecondary or secondary. The polygonal network of interconnected cavities may suggest the partially healed nature of the many of these inclusions and limited time for equilibration of the cavities to attain equilibrium shapes. The fluid influx must have been rapid and copious. Since, these inclusions are certainly of late generation, and also show necking down features, we do not consider the data from these for further discussion.

The distribution pattern of the first category of inclusions within corundum crystals indicates that they were trapped during the growth of the mineral, indicating a 'primary' nature. Linear interconnected 'network' arrays post-date these. Inclusions in both categories belong to the monophase type. Bi-phase or multi-phase inclusions are rare or almost absent. However, some of the inclusions, particularly those in the interconnected irregular network of pseudosecondary category show a bubble at room temperature, which was confirmed as CO_2 (gas) and hence these inclusions have low density CO_2 fluids.

6.2.2. Fluid inclusions in quartz

Quartz from garnet–sillimanite–rutile gneiss (sample K-21) commonly contains fluid inclusions of various shapes, generally ranging in size from 10 to 25 μm. Some inclusions are very small, whereas some have cavities larger than 25 μm. These inclusions are generally rounded, ovoid or diamond-shaped, but some of them have irregular or elongate cavities (hand sketches are given in a later section). These inclusions

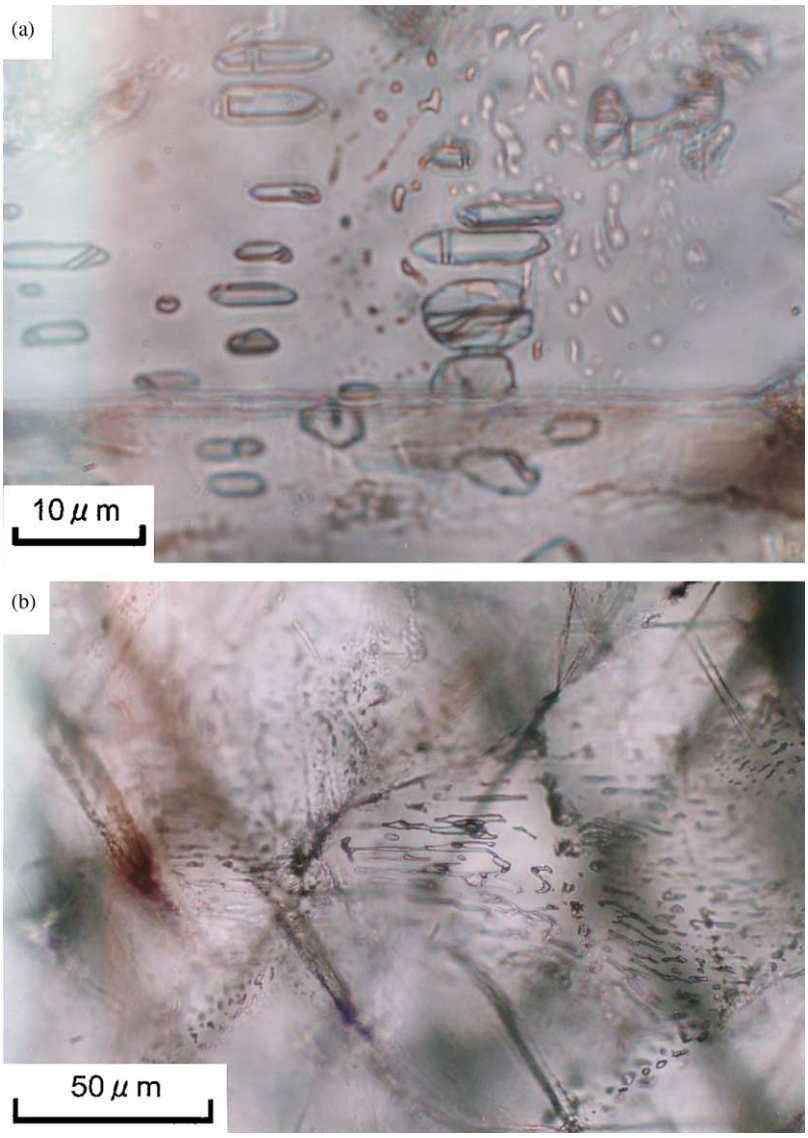

Fig. 4. Photomicrographs of fluid inclusions in corundum from the Bhopalpatnam granulites. (a) Monophase 'primary' CO_2 inclusions in corundum with oval and elongate cavities. (b) Pseudosecondary carbonic inclusions in corundum showing interconnected 'web' of cavities.

form groups or isolated clusters and are classified as 'groups of synchronous inclusions' (GSI) following the scheme proposed by Touret (2001). Most of them are concentrated either towards the center of quartz grains, or in other domains that are away from fractures or cracks. Therefore, these inclusions are considered to be 'primary' and denoted as Group I inclusions.

Some of the groups of inclusions in quartz occur along trails that pinch out within individual grains. These groups of inclusions are smaller than Group I inclusions and sometimes cut across the isolated clusters of Group I type. These inclusions are designated here as Group II, and considered to have been trapped later than Group I inclusions.

Both Groups I and II are monophase at room temperature and are filled with a dense fluid phase. Quartz also contains small bi-phase inclusions essentially along late arrays and microcracks (hand sketches are given in a later section). These inclusions are low temperature aqueous inclusions and do not contain any CO_2. Similar bi-phase inclusions were also observed in feldspar, and are also water-rich with a small vapour bubble. Garnet contains few monophase inclusions, but are too small for microthermometric measurements.

7. Microthermometry

7.1. Analytical procedure

Microthermometric measurements were performed with a LINKAM TH-600 heating–freezing stage at Kochi University. Temperature calibrations were made using natural and synthetic standards of CO_2. The precision of measurements is ± 0.1 °C for freezing data. Fluid inclusions were supercooled using liquid nitrogen and phase changes were observed using a 40× objective. After the fluid is frozen, the inclusions were

Table 3
fluid inclusion micorthermometric data

Host mineral	Melting temperature (oC)			Homogenization temperature (oC)			Molar Volume	Density	Type of
(Rock type)	Min	Max	Peak	Min	Max	Peak	(cc/mol)	(g/cm^3)	inclusion
Corundum (K10-Gneiss)	−58.8	−56.6	−56.8	−18.5	−5.9	−8.5	42.978-45.796	1.024-0.961	Primary
Quartz (Group-I) (K21-Gneiss)	−62.9	−56.6	−58.5	−46.3	−0.1	−2.5	38.579-47.424	1.140-0.928	Primary
Quartz (Group-II) (K21-Gneiss)	−60.3	−56.3	−57.5	0.3	16.2	7.0	47.547-54.290	0.925-0.810	Secondary

warmed slowly at controlled heating rate. After observation of melting temperature, the inclusions were slowly warmed and the homogenization temperatures were carefully observed. Fluid inclusion data were processed using the computer programme, FLINCOR developed by Brown (1989) and the isochores were computed following the equation of state of Holloway (1981).

7.2. Results

Results of microthermometric measurements of fluid inclusions in primary inclusions from corundum crystals and quartz from the gneiss summarized in Table 3, along with computations of molar volumes and density values in terms of CO_2 densities. Sketches of inclusions in corundum analyzed by microthermometry, together with values of melting/homogenization are given in (Fig. 5a and b). Those for monophase inclusions in quartz are given in Fig. 6a and b. Sketches of secondary inclusions in quartz from the gneiss, together with homogenization data are given in Fig. 7. Histogram compiling melting data of monophase inclusions in corundum crystals is given in Fig. 8a, and for quartz from the gneiss is given in Fig. 8b and c. Homogenization data of monophase inclusions in corundum are shown in Fig. 9a and for quartz are given in Fig. 9b and c. The homogenization data from a few secondary low temperature aqueous inclusions are given in Fig. 9d.

Most of the inclusions in corundum crystals showed a sharp peak of melting temperature between −56.6 and −56.8 °C, which is close to the triple point for pure CO_2. Some of the inclusions, however, showed slight depression in melting temperatures down to −58.2 °C, probably indicating traces of impurities such as CH_4 and or N_2, which are known to depress the melting point of pure CO_2. The peak range of melting point temperatures for the primary inclusions in corundum lies between −56.6 and −57.4 °C, indicating that the dominant part of the trapped fluid is pure CO_2.

In quartz from the gneiss, the monophase inclusions show melting temperature in the range of −55.9 to −62.9 °C. The peak range lies between −57 and −59 °C. Clearly, these monophase inclusions contain traces of other volatiles (CH_4/N_2) in addition to CO_2 because the melting point of these inclusions are depressed markedly below the triple point for pure CO_2. This will be further considered in a later section below along with the homogenization data for these inclusions.

When the monophase inclusions are further warmed after first melting, homogenization occurs into liquid phase with shrinking and final disappearance of the gaseous phase. The phase transition was clearly observed in all cases. After homogenization, when the inclusion is cooled again, the bubble reappears, and the homogenization temperature was cross-checked in a number of inclusions and was found to be precisely reproducible.

The lowest homogenization temperature of monophase CO_2 inclusions in corundum is −18.5 °C, and the homogenization temperatures range from −18.5 to −5.9 °C. The relatively low homogenization temperatures assign high densities for the entrapped CO_2 in the range of 1.024–0.961 g/cm^3 with a molar volume of 42.978–45.796 cc/mol.

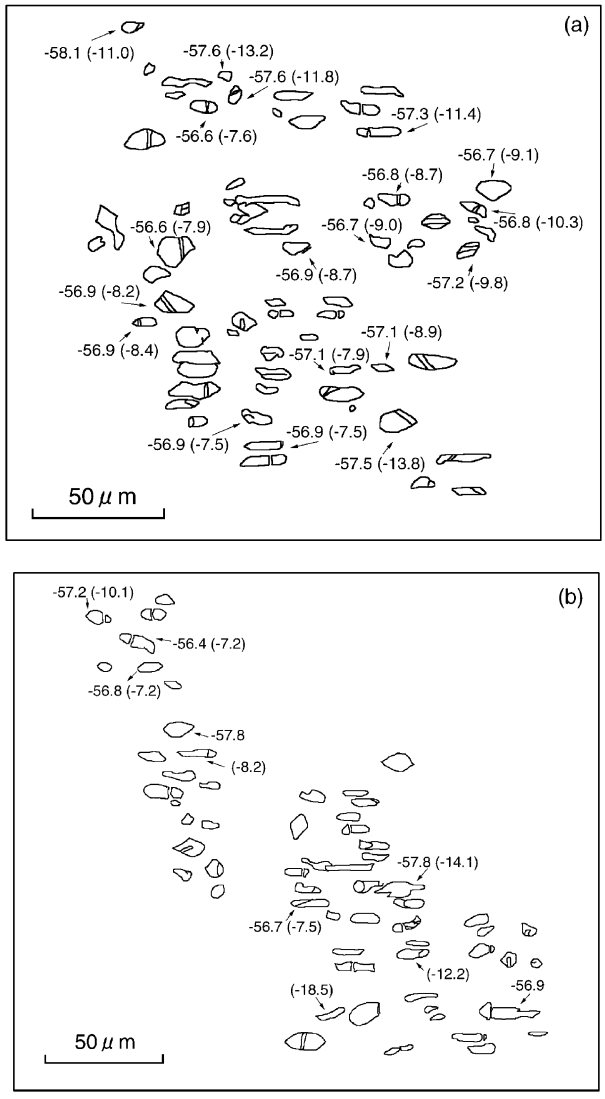

Fig. 5. (a) and (b) Hand sketches of fluid inclusions in corundum from corundum-bearing gneiss with temperatures of melting and homogenization (given inside parantheses) data. The long axes of the inclusions are oriented parallel to the *c*-axis of the crystal.

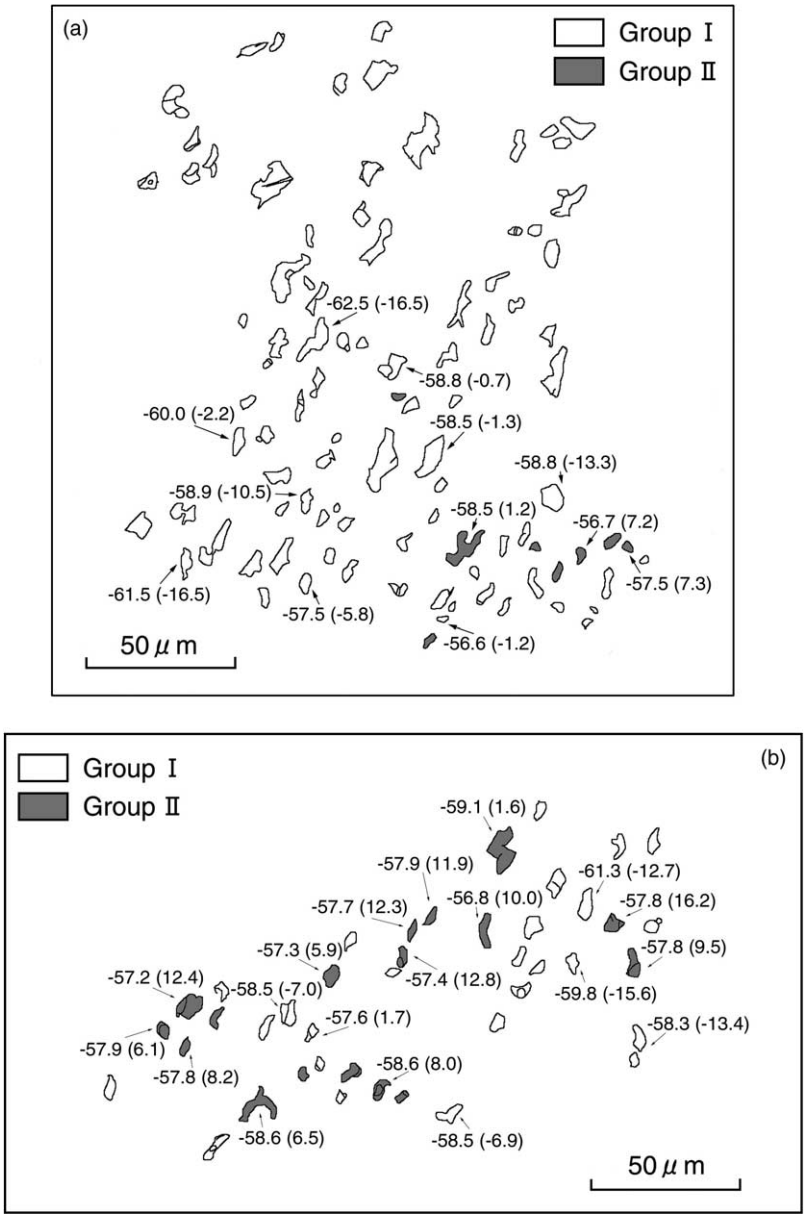

Fig. 6. (a) and (b) Hand sketches of fluid inclusions in quartz from garnet–sillimanite–gneiss showing melting and homogenization (within parentheses) data. Both Groups I and II inclusions are shown.

In quartz from the garnet–sillimanite–rutile gneiss, Group I (primary) inclusions show the lowest homogenization temperature at −46.3 °C, indicating very high density carbonic fluids (1.140 g/cm^3). The homogenization temperature ranges from −46.3 to −0.1 °C for Group I inclusions. Group II inclusions show higher homogenization temperatures of up to 16.2 °C, indicating lower densities.

Fig. 10a shows Tm vs. Th plots of monophase carbonic inclusions in corundum and Fig. 10b shows similar plots of monophase inclusions (Groups I and II) in quartz from the gneiss. It is interesting to note that a definite correlation exists between Tm and Th within inclusions in both cases. Inclusions with maximum depression in melting point temperature show the highest density. Thus, the denser fluids appear to contain additional traces of volatiles. Density of the fluids in these rocks therefore seems to be a function of the composition of the fluid. The relatively lower density fluids are pure CO_2 in all inclusions examined in this study.

In the case of carbonic inclusions in quartz from the pelitic gneiss, the melting temperatures suggest that the entrapped fluid is not pure CO_2 in many cases, because of the melting point depression shown by several inclusions. By combining the melting and homogenization data and by using the curves for CO_2–CH_4 and CO_2–N_2 mixtures, it is possible to make a general estimate of the amount of additional volatiles contained within the inclusion based in the calibrations given by Thiery et al. (1994). If the impurity that depresses the melting temperature is CH_4, then through the intersection of Tm and Th curves in CO_2–CH_4 system, it is possible to estimate a maximum of 18 mol% CH_4 in the fluid. However, if the

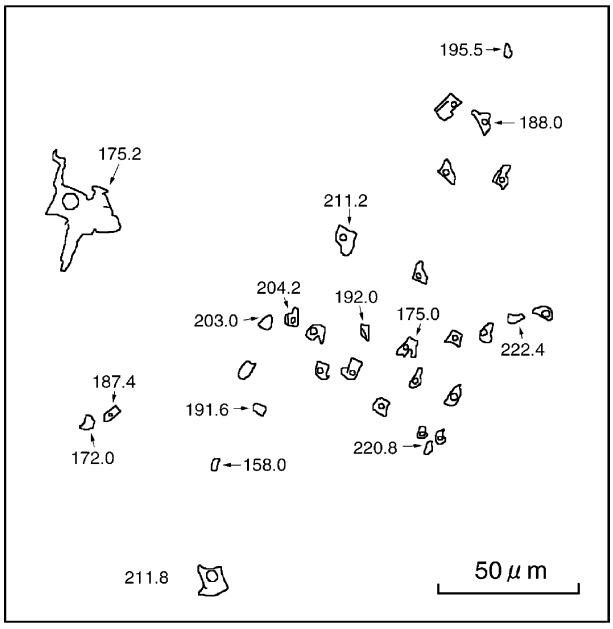

Fig. 7. Hand sketches of bi-phase aqueous inclusions in quartz from garnet–sillimanite–gneiss. The numerical values against each inclusion are homogenization temperatures.

additional volatile that depresses the melting temperature is N_2, then a maximum of about 20 mol% N_2 can be estimated. Since, no Raman spectroscopic data are available on these inclusions, it is difficult to conclude which of the volatiles or volatile mixtures cause the Tm depression. Therefore, for isochore calculations from density data in this study, the fluids are assumed to be near pure CO_2. If CH_4 and/or N_2 are taken into consideration the position of isochores will be shifted slightly towards lower P–T region. We take into consideration this aspect while discussing the slope of the isochores in P–T space in a later section.

Accordingly, the Group I inclusions in quartz from gneiss show very high densities ranging up to 1.140 g/cm^3 (molar volume 38.579 cc/mol). Group II inclusions show low densities of up to 0.810 g/cm^3 (molar volume 54.290 cc/mol).

Late secondary aqueous bi-phase inclusions in quartz and feldspar from the gneiss homogenize into the liquid phase by gradual disappearance of the vapour bubble. The homogenization temperatures show range of 145.5–293.0 °C. Inclusions in feldspar show homogenization between 122.2–162.0 °C. In both cases, the low homogenization temperatures indicate that the fluid inclusions were entrapped from water-rich fluids at low temperature and pressure conditions. They are therefore unrelated to peak metamorphic processes.

Knowledge on the composition and density of a fluid constrain it to lie along an isochore in P–T space. The isochores for pure fluid systems have been constructed from experimental studies (e.g. Thiery et al., 1994) and are available in literature. Isochores can be constructed using density data or molar volume data of fluids. In the present study, the density data have been employed in constructing representative isochores. Fig. 11a shows isochores for CO_2 inclusions in corundum from corundum-bearing gneiss of the study area. Three isochores are shown in the figure indicating the highest, lowest and peak densities. Fig. 11b shows four isochores, the upper two isochore representing the limits of density data from Group I inclusions. The lower two isochores represent the density range for Group II inclusions. It is clear that Group I inclusions have isochores with higher slopes in P–T space as compared to the isochores for Group II inclusions. This indicates that Group I inclusions were entrapped at higher P–T conditions than Group II.

8. Discussion

8.1. Metamorphic P–T history of BGB rocks

Pressure–temperature estimates from the two charnockite samples (K-3 and K-14) based on different methods are compiled in the P–T diagram (Fig. 12). The intersection of the slopes of the pressure estimations from garnet–clinopyroxene–plagioclase–quartz barometry with the temperature estimates from garnet–clinopyroxene and hornblende-plagioclase thermometers defines the peak P–T window of these rocks as 720–800 °C and 8–9.5 kbar (P–T window in Fig. 12 shows the minimum constraints only). This P–T estimate is regarded to represent the peak P–T condition of the BGB. On the other hand, P–T conditions of pelitic gneiss (sample K-21) are defined by the intersection of the P–T ranges of garnet–biotite thermometry and garnet–sillimanite–plagioclase–quartz barometry as 660–720 °C at 4.7–6.5 kbar. The results are slightly lower than those from garnet–bearing charnockite, and probably reflect retrograde event.

As mentioned in a previous section, the garnet–clinopyroxene–plagioclase–quartz assemblage probably preserves near-peak condition because garnet and clinopyroxene are typical minerals in high-grade assemblages. On the other hand, garnet–biotite pairs commonly show later modification of Fe–Mg ratio at lower temperatures, and therefore tend to preserve retrograde condition. We infer that the P–T array of the BGB probably corresponds to a decompressional path along a clockwise exhumation path, although clear reaction textures indicating isothermal decompression could not be observed in this study. Prograde P–T path of the study area is not clearly understood because of the lack of preservation of any prograde mineral assemblages. However, the lower-T and higher-P conditions of 700–740 °C and 7.8–8.4 kbar obtained from garnet–hornblende–plagioclase–quartz assemblages in garnet-bearing charnockite (sample K-14) may be equated to the prograde path, since some hornblendes and plagioclases occur as inclusions in clinopyroxene as earlier phases.

The P–T path that we infer for BGB is in contrast with that proposed by Narasimha et al. (1996) for this terrain. Based on P–T data from charnockite and pelitic gneiss samples, these authors inferred the peak P–T of about 850 °C at 8 kbar, followed by near isobaric cooling toward 600 °C at 7 kbar (the stability field of kyanite). However, Narasimha et al. (1996) do not discuss the procedure of P–T calculations or the basis for

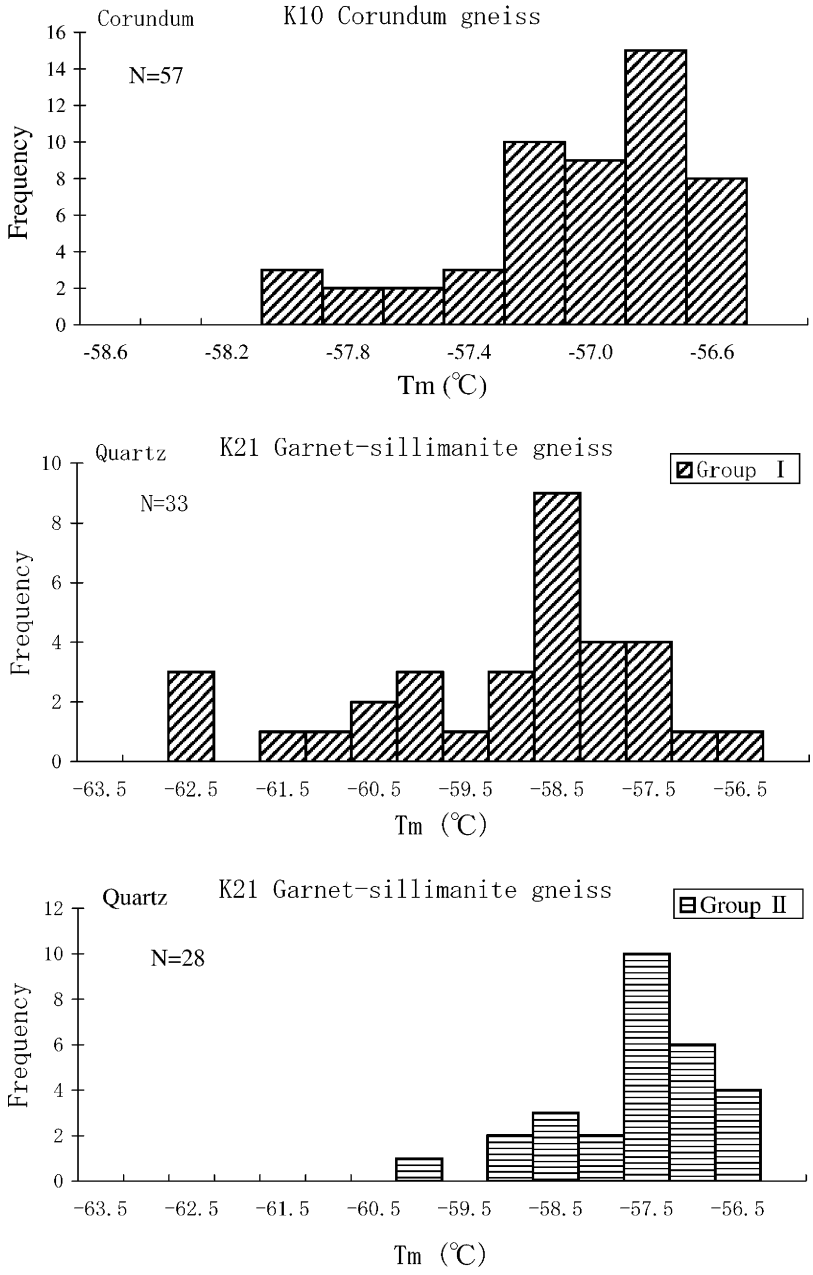

Fig. 8. Histograms showing melting temperatures of fluid inclusions. (a) 'Primary CO_2 inclusions in corundum. (b) Group I inclusions in quartz. (c) Group II inclusions in quartz.

the inferred P–T path. We could not observe any textural evidence for the counterclockwise P–T path proposed by Narasimha et al. (1996). Future studies would resolve this aspect further.

8.2. Metamorphic fluids in BGB

The fluid inclusion data on BGB rocks from our study show the ubiquitous presence of CO_2-rich fluids trapped within various minerals, particularly corundum. The probable presence of traces of additional fluid phases (e.g. CH_4 and/or N_2) is indicated from the depression of CO_2 melting temperatures. A recent fluid inclusion study of ultrahigh-temperature granulites from Tonagh Island in the Napier Complex revealed the occurrence of very high-density CO_2-rich fluids (Tsunogae et al., 2002). Carbonic fluid inclusions commonly present in sapphirine, garnet, orthopyroxene and quartz from Tonagh Island granulites have melting temperatures in the range of −56.3 to −57.2 °C, and homogenization occurs into the liquid phase at temperatures between −34.9 and −4.2 °C. The Th values translate into high densities in the range of 0.9–1.1 g/cm^3. The estimated CO_2 isochores for sapphirine-granulite intersect the counterclockwise P–T trajectory of Tonagh Island rocks at around 6–9 kbar at 1100 °C, which corresponds to the peak metamorphic conditions of the island derived from mineral assemblages, suggesting that the carbonic fluids are traces of syn-metamorphic CO_2 trapped during UHT metamorphism. In other recent studies on high-

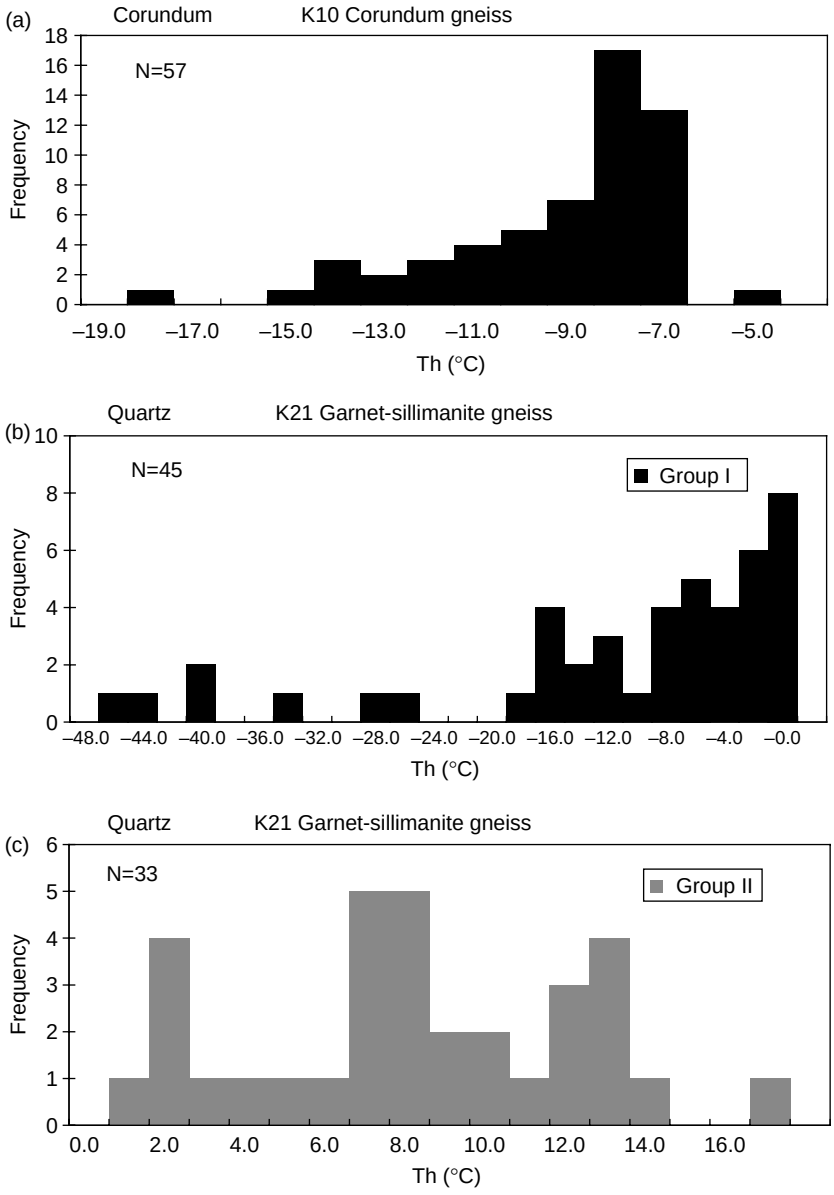

Fig. 9. Histograms showing homogenization temperatures of fluid inclusions. (a) 'Primary' CO_2 inclusions in corundum. (b) Group I inclusions in quartz. (c) Group II inclusions in quartz. (d) Secondary aqueous bi-phase inclusions in quartz.

and ultrahigh-temperature granulites from the Eastern Ghats Belt and the Madurai Block in India (Sarkar et al., 2003; Santosh and Tsunogae, 2003), very high-density CO_2-rich inclusions were reported. These studies illustrated that the high density CO_2-rich fluids were trapped at peak metamorphic conditions. These recent studies emphasize the role of nearly pure CO_2 as the ambient fluid species which buffered water activities and generated the dry granulite assemblages suggesting the role of fluids in extreme crustal metamorphism within the deep crust.

We use Fig. 12 to illustrate the metamorphic and fluid evolution history of the BGB rocks, where the information on fluid inclusion composition and density data have been combined with those from mineral P–T data. In the figure, isochores constructed from CO_2 inclusions in corundum and quartz are shown. Also shown is the box representing the peak temperatures and pressure derived from mineral phase equilibria thermobarometry in the same rock. The P–T box is bound by the isochores for the CO_2 inclusions in corundum. This indicates that the CO_2 in corundum is 'syn-metamorphic', trapped at peak P–T conditions of metamorphism. Thus, the CO_2-rich inclusions in this mineral might represent traces of the original metamorphic fluid.

Isochores from Groups I and II inclusions in quartz from gneiss are also shown in the P–T diagram. Here also, the peak metamorphic P–T field of the rock is bound within the isochores, and the isochores penetrate the P–T box. The highest density isochores, however, passes over the peak P–T field, defining higher pressures and temperatures. However, it was observed that the highest density fluids in quartz show

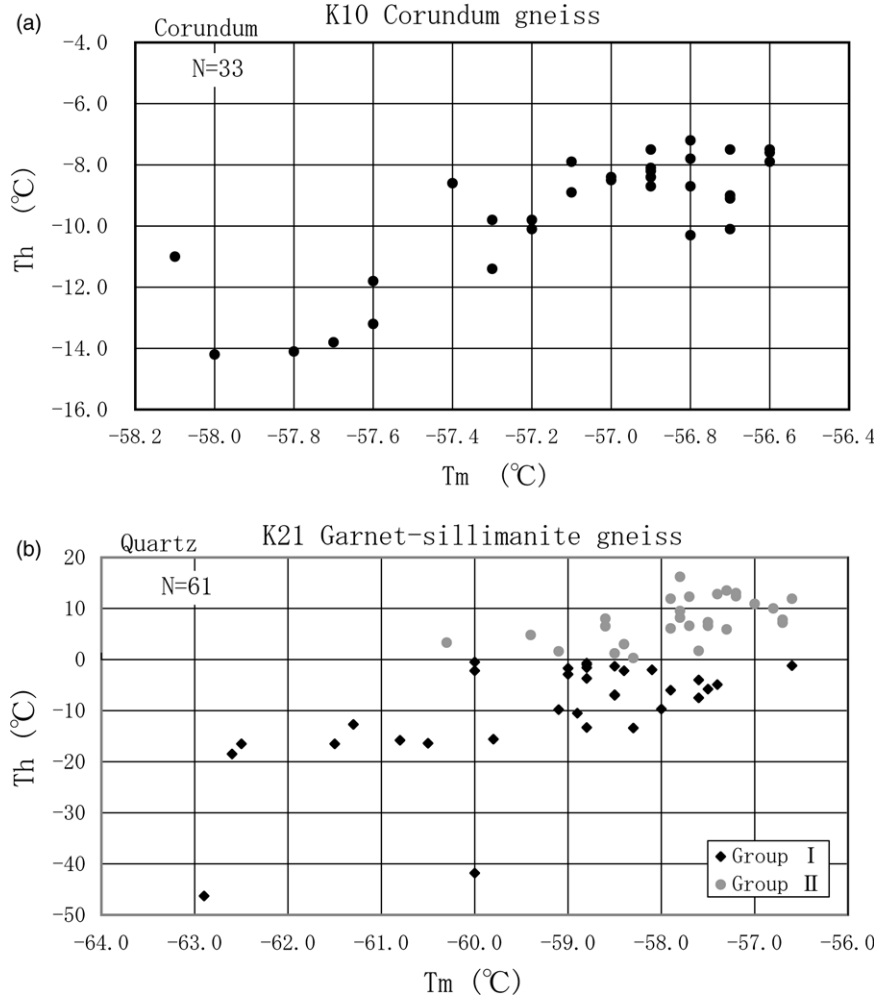

Fig. 10. Homogenization vs. melting temperatures of fluid inclusions. (a) Tm vs. Th plots of CO_2-rich inclusions in corundum. (b) Tm vs. Th plots of Groups I and II inclusions in quartz.

considerable depression in melting temperature, indicating up to 18 mol% CH_4 or up to 20 mol% N_2. If the presence of such additional volatile phases are taken into account, then the position of the isochore would be shifted towards lower slopes, and hence lower P–T conditions. Thus, this isochore would also pass through the peak P–T field. Therefore, it is clear that the high-density inclusions in quartz from the gneiss represent peak metamorphic fluid. The lowest density inclusions define the isochore with the lowest slope in P–T space that does not penetrate through the P–T box, but pass below it. These inclusions are therefore inferred to have been entrapped during uplift, and after peak metamorphism.

No fluid inclusion data have been generated from the charnockites of present study due to the absence of appropriate fluid inclusions for microthermometry in our samples. However, published fluid inclusion data are available for BGB charnockites from the work of Narasimha et al. (1996). The isochores for the major fluid inclusion types in charnockite from their study pass through the P–T boxes defined from mineral thermobarometry of the charnockite in our study. Thus, it is inferred that CO_2-rich fluids were dominant during the peak metamorphism as well as charnockite formation in BGB.

The P–T fields defined from the various thermobarometers broadly overlap. The isochores of CO_2 inclusions in charnockite from the previous study and those for CO_2 inclusions in corundum from the present study define identical slopes and pass through all the P–T boxes. The P–T fields are also found by the isochores for highest and lowest density inclusion in quartz. All the P–T fields and other isochores are enclosed within these two limits. The above features indicate that CO_2-rich fluid inclusions represent traces of the syn-metamorphic fluid, and that granulite formation in BGB witnessed the presence of CO_2-rich fluids, probably derived from fluid-rich magmas emplaced at depth.

The BGB granulites represent part of a Mesoproterozoic mobile belt that was incorporated in a collisional zone between the Bastar and the Dharwar cratons (Santosh et al., 2004). Our study is the first detailed report of fluid regimes in a Mesoproterozoic collisional mobile belt from central India, and shows that CO_2-rich fluids were active in the generation of the granulite facies assemblages. Previously, high density pure

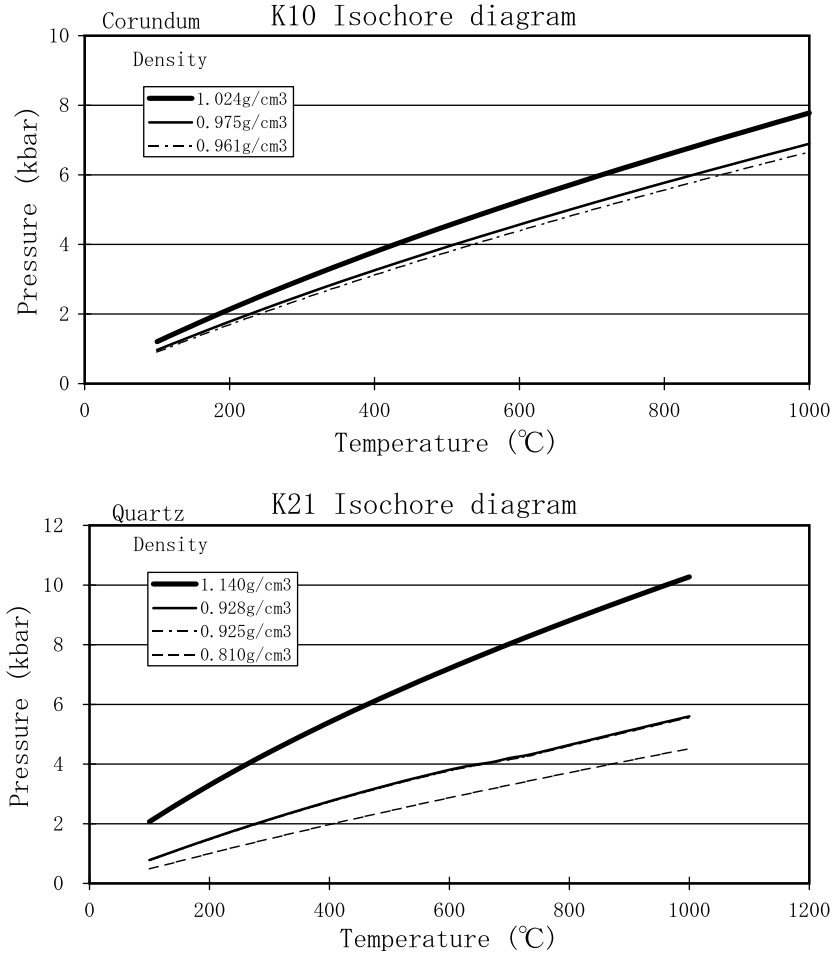

Fig. 11. (a) Isochores for CO_2-rich inclusions in corundum. (b) Isochores for Groups I and II inclusions in quartz.

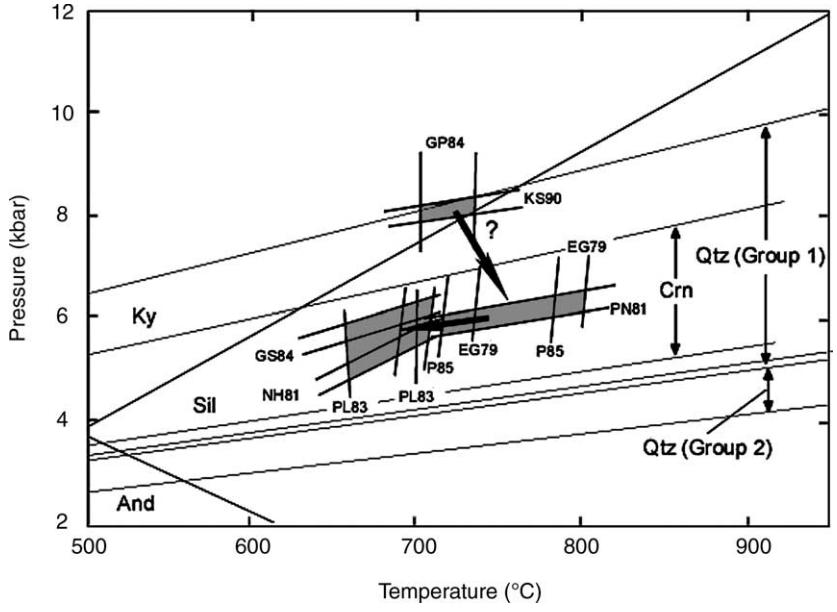

Fig. 12. P–T diagram showing metamorphic conditions estimated from available geothermobarometry in granulites. Shaded areas indicate calculated P–T ranges. Aluminosilicate triple points are after thermodynamic data of Helgeson et al. (1978). Geothermometers: EG79-Ellis and Green (1979), GP84-Graham and Powell (1984), HL77-Holdaway and Lee (1977) P85-Powell (1985), PL83-Perchuk and Lavrent'eva (1983); geobarometers: GS84-Ganguly and Saxena (1984), KS90-Kohn and Spear (1990), NH81-Newton and Haselton (1981), PN81-Perkins and Newton (1981).

CO_2-rich fluids have been reported in Late Archean (Santosh and Tsunogae, 2003) and Pan-African (cf. Santosh, 1992 and references therein) granulites from southern India. Extremely high density carbonic fluids also occur in the Grenvillian ultrahigh temperature metamorphic rocks of the Eastern Ghats Belt (Sarkar et al., 2003). In all these examples, fluid inclusions have been shown to preserve the peak metamorphic fluids. Most granulite terrains in the Precambrian crustal segments are related to major tectonic episodes (e.g. Percival, 1994), and the tectonic processes associated with collision and post-collisional extension during various supercontinental cycles such as Rodinia in the Grenville time and Gondwana during the late Pan-African time (Harley, 1992; Touret and Huizenga, 1999) could have witnessed large scale fluid activity. In some of these cases, the source of the fluids has been traced to sub-continental mantle sources based on stable isotopic studies (cf. Santosh, 1992 and references therein). The source characteristics and mechanism of transfer of the syn-metamorphic CO_2-rich fluids commonly preserved in high grade metamorphic rocks which were generated under different tectonic settings and during various time spans of the earth history remains to be resolved in future studies.

Acknowledgements

Prof. Biswajit Mishra and an anonymous referee provided helpful comments that aided in improving an earlier version of the manuscript. We thank Dr Wilbert Kehelpannala for inviting us to contribute to the special issue. This is a contribution to the research projects led by Prof. M. Arima (Yokohama National University, Japan) and Prof. H. Wada (Shizuoka University, Japan).

References

Acharyya, S.K., 1997. Evolutionary characters of the Gondwanic Indian crust. Indian Minerals 51, 1–24.

Acharyya, S.K., et al., 2000. Comment on 'Crustal structure based on gravity-magnetic modelling constrained from seismic studies under Lambert Rift, Antractica and Godavari and Mahanadi rifts, India and their interrelation ship'. In: Mishra, D.C., et al., (Ed.) Earth and Planetary Science Letters 179, 595–598.

Acharyya, S.K., 2003. The nature of Mesoproterozoic central Indian Tectonic zone with exhumed and reworked older granulites. Gondwana Research 6, 197–214.

Acharyya, S.K., Roy, A., 2000. Tectonothermal history of the central Indian Tectonic zone and reactivation of major fault/shear zones. Journal Geological Society of India 55, 239–256.

Ai, Y., 1994. A revision of the garnet–clinopyroxene Fe^{2+}–Mg exchange geothermometer. Contributions to Mineralogy and Petrology 115, 467–473.

Bolder-Schrijver, L.J.A., Kriegsman, L.M., Touret, J.L.R., 2000. Primary carbonate/CO_2 inclusions in sapphirine-bearing granulites from central Sri Lanka. Journal of Metamorphic Geology 18, 259–269.

Brown, P.E., 1989. FLINCOR—a microcomputer program for the reduction and investigation of fluid inclusions data. American Mineralogist 74, 1390–1393.

Ellis, D.J., Green, D.D., 1979. An experimental study of the effect of Ca upon garnet–clinopyroxene Fe–Mg exchange equilibria. Contributions to Mineralogy and Petrology 71, 13–22.

Frost, B.R., Chacko, T., 1989. The granulite uncertainty principle: limitations on thermobarometry in granulites. Journal of Geology 97, 435–450.

Ganguly, J., Saxena, S.K., 1984. Mixing properties of aluminosilicate garnets: constraints from natural and experimental data, and applications to geothermo-barometry. American Mineralogist 69, 88–97.

Graham, C.M., Powell, R., 1984. A garnet-hornblende geothermometer: calibration, testing, and application to Pelona Schist, southern California. Journal of Metamorphic Geology 2, 13–31.

Harley, S.L., 1992. Proterozoic granulite terranes. In: Condie, K.C. (Ed.), Proterozoic Crustal Evolution Developments in Precambrian Geology, vol. 10. Elsevier, Amsterdam, pp. 301–359.

Helgeson, H.C., Delany, J.M., Nesbitt, H.W., Bird, D.K., 1978. Summary and critique of the thermodynamic properties of rock-forming minerals. American Journal of Science 278-A, 1–229.

Holdaway, M.J., Lee, S.M., 1977. Fe–Mg cordierite stability in high-grade pelitic rocks based on experimental, theoretical, and natural observations. Contributions to Mineralogy and Petrology 63, 175–198.

Holland, T.J.B., Blundy, J.D., 1994. Non-ideal interactions in calcic amphiboles and their bearing on amphibole–plagioclase thermometry. Contributions to Mineralogy and Petrology 116, 433–447.

Holloway, J.R., 1981. Compositions and volumes of supercritical fluids in the earth's crust. In: Hollister, L.S., Crawford, M.L. (Eds.), Fluid Inclusions: Applications to Petrology, vol. 6. Mineralogical Association of Canada, Calgary, pp. 13–38.

Kohn, M.J., Spear, F.S., 1990. Two new geobarometers for garnet amphibolites, with applications to southeastern Vermont. American Mineralogist 75, 89–96.

Kretz, R., 1983. Symbols for rock-forming minerals. American Mineralogist 68, 277–279.

Leake, B.E., Woolley, A.R., Arps, C.E.S., Birch, W.D., Gilbert, M.C., Grice, J.D., Hawthorne, F.C., Kato, A., Kisch, H.J., Krivovichev, V.G., Linthout, K., Laird, J., Mandarino, J.A., Maresch, W.V., Nickel, E.H., Rock, N.M.S., Schumacher, J.C., Smith, D.C., Stephenson, N.C.N., Ungaretti, L., Whittaker, E.J.W., Youzhi, G., 1997. Nomenclature of amphiboles: report of the subcommittee on amphiboles of the international mineralogical association, commission on new minerals and mineral names. American Mineralogist 82, 1019–1037.

Mishra, V.P., Pushkar, S., Dutta, N.K., 1988. Stratigraphy, structure and metamorphic history of Bastar Craton. Records Geological Survey of India 117, 1–26.

Mishra, D.C., Sekhar, D.V.C., Raju, D.C.V., Kumar, V., 1999. Crustal structure based on gravity-magnetic modelling constrained from seismic studies under Lambert rift, Antarctica and Godavari and Mahanadi rifts, India and their interrelationship. Earth and Planetary Science Letters 172, 287–300.

Narasimha, K.N.P., Janardhan, A.S., Mishra, V.P., 1996. Granulites of Bhopalpatnam and Kondagaon belts, bastar craton, M. P: petrological and fluid inclusion studies. Journal of Southeast Asian Earth Sciences 14, 221–229.

Newton, R.C., Haselton, M.T., 1981. Thermodynamics of the garnet-plagioclase-Al_2SiO_5-quartz geobarometer. In: Newton, R.C., Navrotsky, A., Wood, B.J. (Eds.), Thermodynamics of Minerals and Melts. Springer, New York, pp. 131–147.

Newton, R.C., Perkins, D., 1982. Thermodynamic calibration of geobarometers based on the assemblage garnet–plagioclase–orthopyroxene (clinopyroxene)–quartz. American Mineralogist 67, 203–222.

Pattison, D.R.M., Newton, R.C., 1989. Reversed experimental calibration of the garnet–clinopyroxene Fe–Mg exchange geothermometer. Contributions to Mineralogy and Petrology 101, 87–103.

Perchuk, L.L., Lavrent'eva, I.V., 1983. Experimental investigation of exchange equilibria in the system cordierite–garnet–biotite. In: Saxena, S.K. (Ed.), Kinetics and Equilibrium in Mineral Reactions. Springer, New York, pp. 199–239.

Percival, J., 1994. Archean high-grade metamorphism. In: Condie, K.C. (Ed.), Proterozoic Crustal Evolution Developments in Precambrian Geology, vol. 10. Elsevier, Amsterdam, pp. 301–359.

Perkins, D., Newton, R.C., 1981. Charnockite geobarometers based on coexistence garnet–pyroxene–plagioclase–quartz. Nature 292, 144–146.

Powell, R., 1985. Regression diagnostics and robust regression in geothermometer/geobarometer calibration: the garnet–clinopyroxene geothermometer revisited. Journal of Metamorphic Geology 3, 231–243.

Radhakrishna, B.P., Naqvi, S.M., 1986. Precambrian continental crust of India and its evolution. Journal of Geology 94, 145–166.

Rajesham, T., Bhaskar Rao, Y.J., Murthi, K.S., 1993. The Karimnagar granulite terrane—a new sapphirine bearing granulite province, south India. Journal Geological Society of India 41, 51–59.

Ramachandra, H.M., Roy, A., Mishra, V.P., Dutta, N.K., 2001. A critical review of the tectonothermal evolution of the Bastar Craton. Proc. M.S. Krishnan Centenary Commemorative National Seminar, Geological Survey of India Special Publication, vol. 55, pp. 161–180.

Roedder, E., 1984. Fluid inclusions. Review in Mineralogy (Mineralogical Society of America), vol. 12, 644pp.

Rogers, J.J.W., Santosh, M., 2002. Configuration of Columbia, a Mesoproterozoic supercontinent. Gondwana Research 5, 5–22.

Rogers, J.J.W., Santosh, M., 2003. Supercontinents in earth history. Gondwana Research 6, 357–368.

Santosh, M., 1992. Carbonic fluids in granulites: cause or consequence? Journal Geological Society of India 39, 375–399.

Santosh, M., Tsunogae, T., 2003. Extremely high density pure CO_2 fluid inclusions in a garnet granulite from southern India. Journal of Geology 111, 1–16.

Santosh, M., Jackson, D.H., Harris, N.B.W., Mattey, D.P., 1991. Carbonic fluid inclusions in south India granulites: evidence for entrapment during charnockite formation. Contributions to Mineralogy and Petrology 108, 318–330.

Santosh, M., Tagawa, M., Taguchi, S., Yoshikura, S., 2003. The Nagercoil granulite block, southern India: petrology, fluid inclusions and exhumation history. Journal of Asian Earth Sciences 22, 131–155.

Santosh, M., Yokoyama, K., Acharyya, S.K., 2004. Geochronology and tectonic evolution of Karimnagar and Bhopalpatnam granulite belts, central India. Gondwana Research 7, 501–518.

Sarkar, S., Santosh, M., Dasgupta, S., Fukuoka, M., 2003. Very high density CO_2 associated with ultrahigh-temperature metamorphism in the eastern Ghats granulite belt, India. Geology 31, 51–54.

Sengupta, P., Dasgupta, S., Bhattacharya, P.K., Pariya, Y., 1989. Mixing behavior in quaternary garnet solid solution and an extended Ellis and Green garnet–clinopyroxene geothermometer. Contributions to Mineralogy and Petrology 103, 223–227.

Thiery, R., Van den Kerkhof, A.M., Dubessy, J., 1994. V-X properties of CH_4–CO_2 and CO_2–N_2. Modelling for fluid inclusions ($T<31$ °C; $P<400$ bar). European Journal of Mineralogy 6, 753–771.

Touret, J.L.R., 1985. Fluid regime in southern Norway, the record of fluid inclusions. In: Tobi, A.C., Touret, J.L.R. (Eds.), The Deep Proterozoic Crust in the North Atlantic Provinces. Reidel, Dordrecht, pp. 517–549.

Touret, J.L.R., 2001. Fluids in metamorphic rocks. Lithos 55, 1–26.

Touret, J.L.R., Hansteen, T.H., 1988. Geothermobarometry and fluid inclusions in a rock from the Doddabetta charnockite complex, southwest India. Ren Society Ital Mineral Petrol 43, 65–82.

Touret, J.L.R., Huizenga, J.M., 1999. Precambrian intraplate magmatism: high temperature, low pressure crustal granulites. Journal of African Earth Sciences 28, 367–382.

Tsunogae, T., Santosh, M., Osanai, Y., Owada, M., Toyoshima, T., Hokada, T., 2002. Very high-density carbonic fluid inclusions in sapphirine-bearing granulites from Tonagh island in the Archean Napier complex, east Antarctica: implications for CO_2 infiltration during ultrahigh-temperature ($T>1100$ °C) metamorphism. Contributions to Mineralogy and Petrology 143, 279–299.

Van den Kerkhof, A.M., Hein, U.F., 2001. Fluid inclusion petrography. Lithos 55, 27–47.

Yedekar, D.B., Jain, S.C., Nair, K.K.K., Dutta, K.K., 1990. Central Indian collision suture. Geological Survey of India Special Publication 29, 1–43.